The Astrophysical Journal, 665:1428–1438, 2007 August 20

A COMPARATIVE STUDY BETWEEN ERUPTIVE X-CLASS FLARES ASSOCIATED WITH CORONAL MASS EJECTIONS AND CONFINED X-CLASS FLARES

Yuming Wang[1,2] and Jie Zhang[1]
Received 2007 March 16; accepted 2007 May 9

ABSTRACT

We examine the two kinds of major energetic phenomena that occur in the solar atmosphere: eruptive and confined events. The former describes flares with associated coronal mass ejections (CMEs), while the latter denotes flares without associated CMEs. We find that about 90% of X-class flares are eruptive, but the remaining 10% are confined. To probe why the largest energy releases could be either eruptive or confined, we investigate four X-class events from each of the two types. Both sets of events are selected to have very similar intensities (X1.0 to X3.6) and duration (rise time under 13 minutes and decay time over 9 minutes) in soft X-ray observations, to reduce any bias due to flare size on CME occurrence. We find that the occurrence of eruption (or confinement) is sensitive to the displacement of the location of the energy release, defined as the distance between the flare site and the flux-weighted magnetic center of the source active region. The displacement is 6–17 Mm for confined events but as large as 22–37 Mm for eruptive events. This means that confined events occur closer to the magnetic center, while the eruptive events tend to occur close to the edge of active regions. We use the potential field source-surface model to infer the coronal magnetic field above the source active regions and calculate the flux ratio of low ($<1.1\ R_\odot$) to high ($\geq 1.1\ R_\odot$) corona. We find that the confined events have a lower ratio (<5.7) than the eruptive events (>7.1). These results imply that a stronger overlying arcade field may prevent energy releases in the low corona from being eruptive, resulting in flares, but without CMEs.

Subject headings: Sun: coronal mass ejections (CMEs) — Sun: flares — magnetic fields

1. INTRODUCTION

Coronal mass ejections (CMEs) and flares are known to be the two most energetic phenomena that occur in the atmosphere of the Sun, and they have profound effects on the geospace environment and human technological systems. In this paper, we intend to examine the physical origins of CMEs and flares by comparatively studying two different kinds of energetic phenomena, both of which have almost identical flares; however, one is associated with CMEs and the other is not. Before the advent of direct CME observations, these two kinds of phenomena were referred to as eruptive flares and confined flares, respectively (e.g., Švestka & Cliver 1992). An eruptive flare (also called a dynamic flare) usually appears as having two ribbons and postflare loops in Hα imaging observations and is of long duration (e.g., tens of minutes up to hours) in soft X-rays, while a confined flare occurs in a compact region and lasts for only a short period (e.g., minutes). Following this convention, but without trying to imply a causal relation between flares and CMEs, hereafter we refer to a flare associated with an observed CME as an "eruptive event," and a flare not associated with a CME as a "confined event."

It has been suggested based on observations that CMEs and flares are two different manifestations of the same energy release process in the corona (e.g., Harrison 1995; Zhang et al. 2001; Harrison 2003). They do not drive one another but are closely related. In particular, Zhang et al. (2001, 2004) showed that the fast acceleration of CMEs in the inner corona coincides very well in time with the rise (or energy release) phase of the corresponding soft X-ray flares, strongly implying that both phenomena are driven by the same process at the same time, possibly by magnetic field reconnections. However, this implication raises another important question, that of under what circumstances the energy release process in the corona leads to an eruption, and under what circumstances confinement prevails during the process. An answer to this question will shed light on the origin of flares as well as CMEs.

The rate of occurrence of eruptive events depends on the intensity and duration of flares. A statistical study performed by Kahler et al. (1989) has shown that longer duration flares tend to be eruptive, while more impulsive flares tend to be confined. By using CME data from the *Solar Maximum Mission* (*SMM*) and flare data from the *Geostationary Operational Environmental Satellites* (*GOES*) from 1986 to 1987, Harrison (1995) found that the association ratio of flares with CMEs increases from about 7% to 100% as the flare class increases from B to X, and from about 6% to 50% as the flare duration increases from about 1 to 6 hours. Andrews (2003) examined 229 M- and X-class X-ray flares during 1996–1999 and found that the CME association rate, or eruption rate, is 55% for M-class flares and 100% for X-class flares. With a much lager sample of 1301 X-ray flares, Yashiro et al. (2005) obtained a similar result, finding the eruption rates of C-, M-, and X-class flares to be 16%–25%, 42%–55%, and 90%–92%, respectively. Yashiro et al.'s (2005) work showed that a flare will not necessarily be associated with a CME even if it is as intense as an X-class flare. Such confined but extremely energetic events have also been reported by Feynman & Hundhausen (1994) and Green et al. (2002).

The studies mentioned above indicate the probability of CME occurrence for a given flare. On the other hand, there is also a probability of flare occurrence for a given CME. There are CMEs that may not necessarily be associated with a noticeable X-ray flare. Zhang et al. (2004) reported an extremely gradually accelerated slow CME without any flare association, implying that nonflare eruptive events tend to be slowly driven. By combining coronal data from *SMM* and 6 hr soft X-ray data from *GOES*,

[1] Department of Computational and Data Sciences, College of Science, George Mason University, Fairfax, VA 22030; ywangf@gmu.edu, jzhang7@gmu.edu.

[2] School of Earth and Space Sciences, University of Science and Technology of China, Hefei, 230026 Anhui, China; ymwang@ustc.edu.cn.

St. Cyr & Webb (1991) reported that about 48% of front-side CMEs were associated with X-ray events near the minimum of solar cycle 21. Based on observations with the *Solar and Heliospheric Observatory* (*SOHO*), Wang et al. (2002) studied 132 front-side halo CMEs and found that the association rate of CMEs with X-ray flares stronger than C class increased from 55% at solar minimum to 80% near solar maximum. With 197 halo CMEs identified during 1997–2001, Zhou et al. (2003) concluded that 88% of CMEs were associated with brightenings in the extreme-ultraviolet (EUV).

Some attempts have been made to explain the confinement or the eruptiveness of a solar energetic event in the context of the configuration of the coronal magnetic field. Green et al. (2002) analyzed the 2000 September 30 confined event, utilizing multiwavelength data, and suggested that it involved magnetic reconnection of two closed loops to form two new closed loops without any opening of the involved magnetic structure. Nindos & Andrews (2004) carried out a statistical study of the effect of magnetic helicity on eruption rate. They found that the coronal helicity of active regions that produce confined events tends to be smaller than the helicity of those that produce eruptive events.

In this paper, we approach the eruption-confinement issue in solar energetic events with a comparative study. We focus on the most energetic confined events, those that produce X-class soft X-ray flares but not CMEs. While the majority of X-class flares are eruptive, a small fraction (about 10%) of them are confined. The magnetic properties of these confined events should stand out more than those of less energetic confined events. To make an effective comparison, we select eruptive events with X-ray properties, in terms of intensity and duration, that are very similar to those of the selected confined events. The differences in magnetic configuration between these two sets of events will most likely reveal the true causes of eruption or confinement. How we select the events and their basic properties are described in § 2. Detailed comparative analyses of the two sets of events are given §§ 3 and 4, which focus on the properties of the photospheric magnetic field distribution and the extrapolated coronal magnetic field distribution, respectively. In § 5, we summarize.

2. SELECTION OF EVENTS AND OBSERVATIONS

2.1. *Confined Events: X-Class Flares without CMEs*

From 1996 to 2004, there were 104 X-class soft X-ray flares reported by the NOAA Space Environment Center. The flares are recorded by high temporal resolution (every 3 s) *GOES* measurements of the disk-integrated soft X-ray flux in two passbands, 1.0–8.0 Å and 0.5–4.0 Å. The flare catalog provides the peak intensity, beginning time, peak time, and ending time of flares. Based on peak intensity, flares are classified into five categories: A, B, C, M, and X, in order of increasing strength. An X-class flare, in the strongest category, is defined by a peak flux in the 1.0–8.0 Å band exceeding 10^{-4} W m^{-2}.

To find out whether a flare is associated with a CME or not, we make use of both the CME observations by the Large Angle and Spectrometric Coronagraph (LASCO; Brueckner et al. 1995) and coronal disk observations by the EUV Imaging Telescope (EIT; Delaboudinière et al. 1995); both instruments are on board the *SOHO* spacecraft. The search process started with the LASCO CME catalog (Yashiro et al. 2004)[3] for an initial quick look. A flare became a candidate confined event if there was not any CME whose extrapolated onset was within a 60 minute window centered on the flare onset time. The time of onset of a CME is calculated by linearly extrapolating the height-time measurement in the outer corona back to the surface of the Sun, which should provide a first-order approximation of the true onset time of the CME. Further, we visually examined the sequence of LASCO and EIT images around the flare time to verify that indeed there was no CME associated with the flare under study. One property in common to these confined events is a lack of EUV dimming in EIT images, even though they do show strong compact brightenings. Following the compact brightening, there is no corresponding CME feature that appears in subsequent LASCO images. This scenario is in sharp contrast to that of an eruptive event, in which an EIT dimming accompanies the brightening and, within a few frames, a distinct CME feature appears in the appropriate position angle in LASCO images. After applying this process to all of the X-class flares, we found 11 events that are confined; they are listed in Table 1. We note that events 7–11 occurred within 3 days between 2004 July 15 and 17, and they all originated from the same solar active region (NOAA AR 10649).

Among the 11 confined X-class flares from 1996 to 2004, the first four events have been reported on earlier by Yashiro et al. (2005). The third one was also reported on and studied by Green et al. (2002). During 1996–2004, there were in total 104 X-class flares. Thus, the percentage of confined X-class flares is about 10%. As shown in Table 1, all these confined flares were impulsive. Their rise times do not exceed 13 minutes, except for event 8 (23 minutes). The decay time does not exceed 10 minutes for any of the 11 events. The rise and decay times are derived from the beginning, maximum, and ending times of the flares, which are defined and compiled by the Space Environment Center.[4] The peak intensity of all these events was below the X2.0 level, except for event 10 (X3.6). Events stronger than X3.6 were found to always be associated with a CME.

Out of the 11 confined events, we were able to select four that are suitable for further in-depth analysis. These are events 4, 5, 6 and 11. They are suitable because (1) the flare is isolated, which means that there was no other flare immediately preceding or following, and (2) there is no other coronal dimming or CME eruption in the vicinity of the flare region within a certain period. Events 1 and 3 were not selected because they were mixed up with a flare-CME pair from the same source region. In the presence of an eruptive flare immediately preceding or following a confined event, we are not certain to what extent the confined event is related to the earlier or later eruptive one. In order to make our analysis as "clean" as possible, such events were discarded. Event 2 was also excluded, because its source region is right behind the western limb, and hence no timely magnetogram data are available. Events 7 through 11 were all from the same active region. By overplotting EIT images showing flare locations on the *SOHO* Michelson Doppler Imager (MDI) magnetogram images, we find that these flares essentially occurred at the same location within the active region. Thus, we chose only the last event to represent all five. The four confined events selected for further analysis are labeled C_1 through C_4 in the second column of Table 1.

2.2. *Eruptive Events: X-Class Flares with CMEs*

For comparison with the four confined events mentioned above, a set of four eruptive X-class flares were selected. These were chosen to have similar properties in X-rays to the confined events: (1) their rise and decay times are less than 13 minutes, and

[3] The NRL-GSFC-CUA CME catalog at http://cdaw.gsfc.nasa.gov/CME_list.

[4] See http://www.sec.noaa.gov/ftpdir/indices/events/README.

TABLE 1

CONFINED X-CLASS FLARES FROM 1996 TO 2004 AND SELECTED ERUPTIVE FLARES

No.	Label	Date	Beginning (UT)	T_R[a] (minutes)	T_D[b] (minutes)	Class	Location	NOAA AR	CME V/Width[c]	Comment
					Confined Flares					
1.....	...	2000 Jun 6	13:30	9.0	7.0	X1.1	N20, E18	9026	...	Contained by a preceding and a following M-class flare (Y)
2.....	...	2000 Sep 30	23:13	8.0	7.0	X1.2	N07, W91	9169	...	Limb event (G, Y)
3.....	...	2001 Apr 2	10:04	10.0	6.0	X1.4	N17, W60	9393	...	Contained by a preceding eruptive flare (Y)
4.....	C_1	2001 Jun 23	04:02	6.0	3.0	X1.2	N10, E23	9511	...	(Y)
5.....	C_2	2003 Jun 9	21:31	8.0	4.0	X1.7	N12, W33	10374	...	
6.....	C_3	2004 Feb 26	01:50	13.0	7.0	X1.1	N14, W14	10564	...	
7.....	...	2004 Jul 15	18:15	9.0	4.0	X1.6	S11, E45	10649	...	
8.....	...	2004 Jul 16	01:43	23.0	6.0	X1.3	S11, E41	10649	...	
9.....	...	2004 Jul 16	10:32	9.0	5.0	X1.1	S10, E36	10649	...	
10.....	...	2004 Jul 16	13:49	6.0	6.0	X3.6	S10, E35	10649	...	
11.....	C_4	2004 Jul 17	07:51	6.0	2.0	X1.0	S11, E24	10649	...	Events 7–11 all from the same AR
					Eruptive Flares					
1.....	E_1	1998 May 2	13:31	11.0	9.0	X1.1	S15, W15	8210	936/halo	
2.....	E_2	2000 Mar 2	08:20	8.0	3.0	X1.1	S18, W54	8882	776/62°	
3.....	E_3	2000 Nov 24	04:55	7.0	6.0	X2.0	N19, W05	9236	1289/halo	
4.....	E_4	2004 Oct 30	11:38	8.0	4.0	X1.2	N13, W25	10691	427/halo	

[a] Rise time of the flare.

[b] Decay time of the flare.

[c] Apparent speed (km s^{-1}) and angular width of CMEs. Adopted from the online GSFC-NRL-CUA CME catalog. "G" and "Y" in the comment column mean that the corresponding event was reported on by Green et al. (2002) or Yashiro et al. (2005), respectively.

(2) their intensities are between X1.0 and X2.0. Furthermore, their locations are within 60° in longitude from the solar central meridian, in order to reduce projection effects in the magnetograms. These flares, which are relatively impulsive, are indeed associated with CMEs, as shown in LASCO images. These four events are also listed in Table 1, labeled E_1 through E_4.

An overview of the two sets of events is given in Figure 1. The top shows the four confined events, and the bottom shows the four eruptive events. For each event, we show the *GOES* soft X-ray flux profile (all for a 2 hr interval), the running-difference EIT image, and a running-difference LASCO image in the upper, middle, and lower panels, respectively. It is apparent that the temporal profiles of the *GOES* soft X-ray fluxes exhibit no noticeable difference between the two sets of events, because of the constraint on our selection of events. Moreover, as seen in the EIT images, the two sets of events are all associated with compact coronal brightening, indicating the occurrence of a flare. However, for the eruptive flares the accompanying CMEs are clearly seen in the LASCO images. In contrast, there is no apparent brightening (CME) feature seen in the LASCO images for the confined events (only one image is shown here to represent the observed sequence of images, which all indicate an undisturbed corona). For the eruptive events, the speeds and angular widths of the CMEs are also listed in Table 1.

3. MAGNETIC PROPERTIES IN THE PHOTOSPHERE

3.1. *Flare Location and Active Region Morphology*

To explore what physical factors led to the two similar sets of flares, all strong and impulsive, having differences in CME production, we first study the magnetic properties of their surface source regions. The *SOHO* MDI instrument provides observations of the photospheric magnetic field (the component along the line of sight) every 96 minutes. The spatial resolution of MDI magnetograms is about 4″ with a plate scale of 2″ pixel^{-1}, at which level detailed magnetic features across the source active regions are reasonably resolved. To reduce the effect of projecting the line-of-sight magnetic field, we have chosen only events within 60° of the solar central meridian.

For each event, we determined the location of the flare seen by EIT relative to the magnetic features seen by MDI. We first aligned the MDI image with the corresponding EIT image. The differences in timing between MDI and EIT images have been taken into account. Figure 2 illustrates the alignment for the 2001 June 23 event. The soft X-ray flare began at 04:02 UT and peaked at 04:09 UT. An EIT 195 Å image showing the flare was taken at 04:11 UT. The nearest full-disk MDI image prior to the flare was taken at 03:11 UT. The MDI magnetogram was rotated to fit the EIT time and then superposed as contours onto the EIT image. In the right panel of Figure 2, we display the aligned images; only the region of interest is shown. Using this method, we are able to determine the location of the flare, which is just above the neutral lines seen in the magnetogram.

Figures 3 and 4 show the magnetograms for the four confined events and the four eruptive events, respectively. The flare sites, or bright patches seen in EIT images, are marked with red asterisks in the images. The magnetogram images have been remapped onto the Carrington coordinates, which reduces the effect of spherical projection of the image area. The x-axis is the Carrington longitude in degrees, and the y-axis is the sine of latitude. The images shown in Figures 3 and 4 are all 30° × 30° square, which usually covers the entire active region producing the CME or flare of interest. To highlight the magnetic features, the displayed images have been segmented into three different levels: strong positive magnetic field (≥50 G, *white*), strong negative magnetic field (≤−50 G, *black*), and weak field (from −50 to 50 G, *gray*). Note that the noise level of an MDI magnetogram image is typically about 10 G. As shown in the figures, an active region naturally segments into many individual pieces. Those with magnetic flux higher than 10^{13} Wb are labeled by a letter with a number in parentheses indicating the magnetic flux in units of 10^{13} Wb.

3.2. *Results*

We find that there is no apparent difference in terms of total magnetic flux of the source regions between the confined events and eruptive events. The total magnetic fluxes, combining both positive and negative values, are listed in Table 2. The total flux for confined events varies from about 5×10^{13} to 36×10^{13} Wb, while for eruptive events it varies from about 11×10^{13} to 24×10^{13} Wb.

However, there is a noticeable pattern, in that the confined flares all originate in a location relatively close to the center of the host active region. Figure 3*a* shows the confined event of 2001 June 23. There are three relatively large magnetic regions, labeled A, B, and C. The flare site is surrounded by regions A and B. Figure 3*b* shows the 2003 August 9 confined event. The flare location is associated with three small negative patches (*red asterisks*) embedded in the large positive piece A. Figure 3*c* shows the 2004 February 26 confined event. The flare occurred just above the neutral line between the large positive region A and the large negative piece B. Figure 3*d* shows the 2004 July 17 confined event. The flare was located in a complex active region with a large number of sunspots. It occurred right at the boundary between pieces C and F. From the view of the entire active region, C and F were further enclosed by two much larger and stronger pieces, A and D, whose fluxes were about 10 times larger.

For the eruptive flares, on the other hand, the flare sites were all relatively far from the center of the magnetic flux distribution. In other words, they were closer to the edge of the hosting active region. Figure 4*a* shows the 1998 May 2 event. The strongest pair of magnetic pieces are A and D, but the eruptive flare occurred at the neutral line between D and piece C, which is the smallest among the four labeled regions in the active region. Figure 4*b* shows the 2000 March 2 event. Similarly, the strongest pair of pieces were A and C, but the flare was from the neutral line between C and piece B, which is the smallest labeled region. Figure 4*c* shows the 2000 November 24 event. The flare occurred at the outer edge of the strongest piece, A, which was neighbored by a very small region with negative flux. Figure 4*d* shows the 2004 October 30 event. The flare site was also close to the edge of the entire active region.

To quantify this observation of different displacements in flare location, we introduce a flare displacement parameter, which is defined by the surface distance between the flare site and the weighted center of the magnetic flux distribution of the host active region, or center of magnetic flux (COM) for short. The COM might be the place that has the most overlying magnetic flux. The COM is calculated based on the remapped 30° × 30° MDI images (without segmentation). It is a point across which any line can split the magnetogram into two flux-balanced halves and can be formulated as $x_c = \sum_i F_i x_i / \sum_i F_i$ and $y_c = \sum_i F_i y_i / \sum_i F_i$. The COMs of these events are marked by diamonds in Figures 3 and 4. With a known COM, it is easy to derive the displacement parameter, which is listed in Table 2. Consistent with the earlier discussion, it is found that the displacement parameters for the four confined events are all smaller than 17 Mm, while for the four eruptive events they are all larger than 22 Mm.

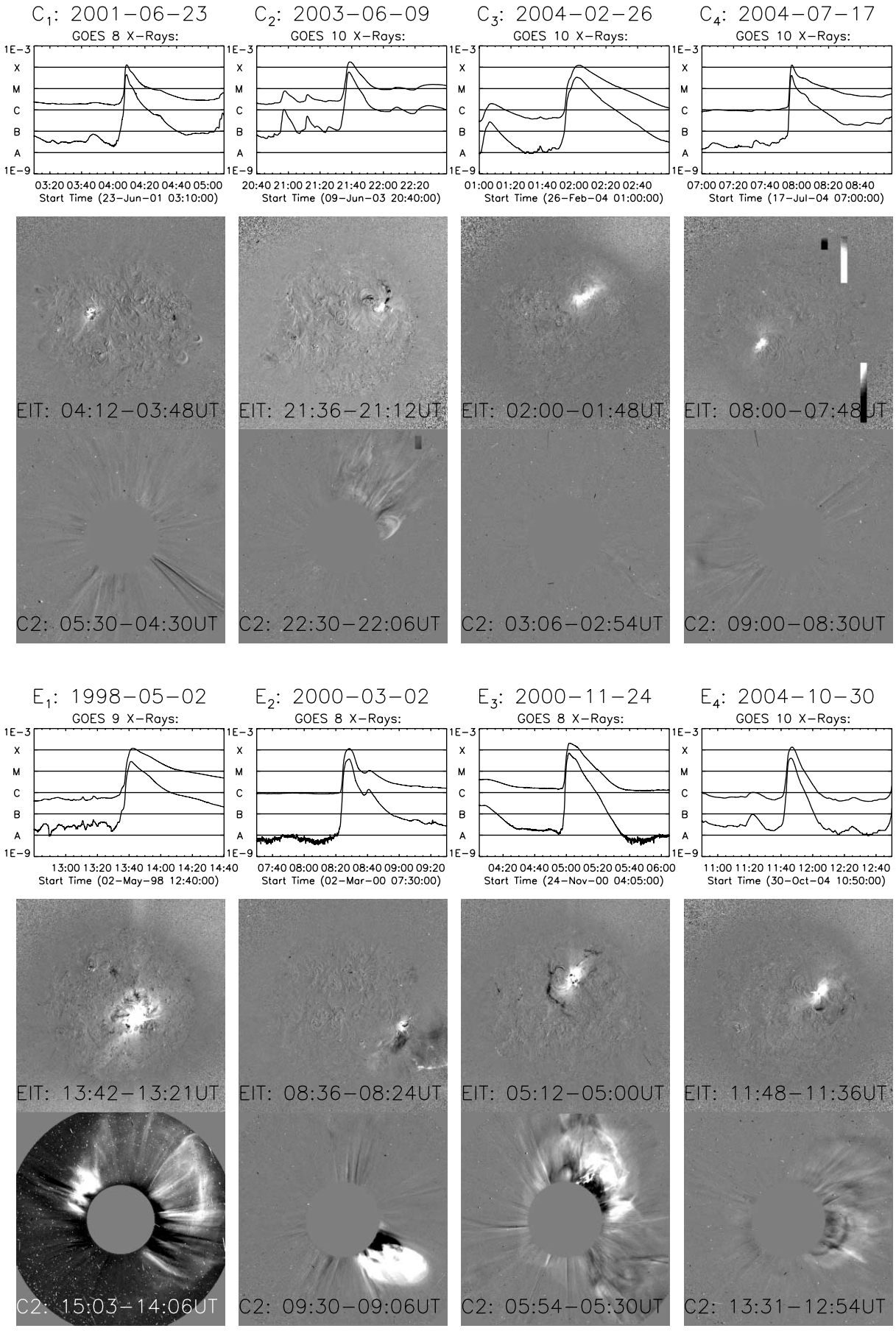

FIG. 1.— Overview of the four confined (C_1–C_4, *top*) and four eruptive (E_1–E_4, *bottom*) flares. For each event, we display the *GOES* X-ray flux profile (spanning 2 hr) and running-difference EIT 195 Å and LASCO/C2 images in the three panels from top to bottom.

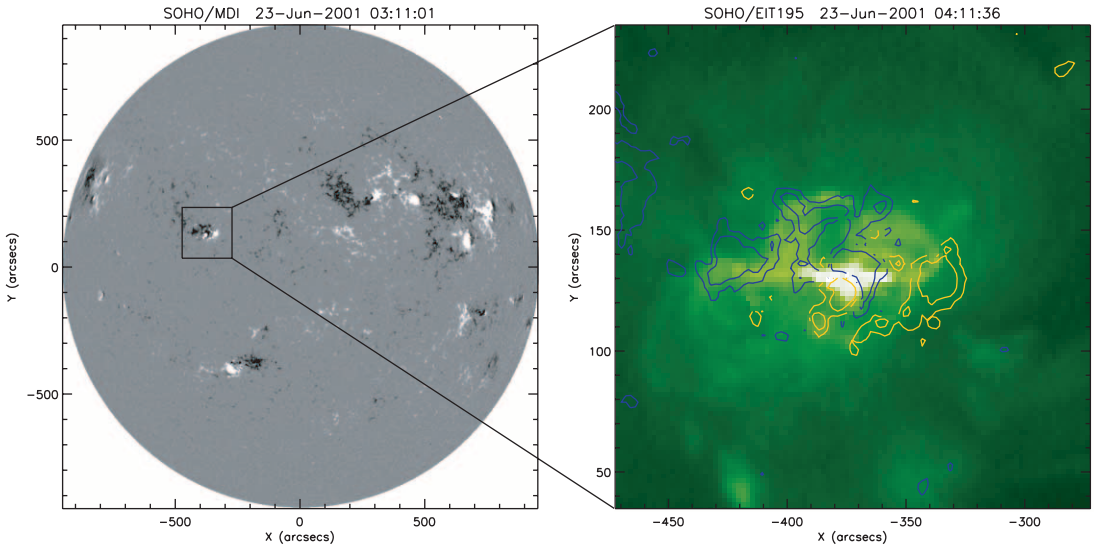

FIG. 2.— Example showing a flare and its source region. The left image is a full-disk MDI magnetogram taken before the flare's onset. The right image shows the EIT image in green-and-white false color; the white patch at the center denotes the flare location. The superposed contours show the magnetogram, with yellow the positive and blue the negative field.

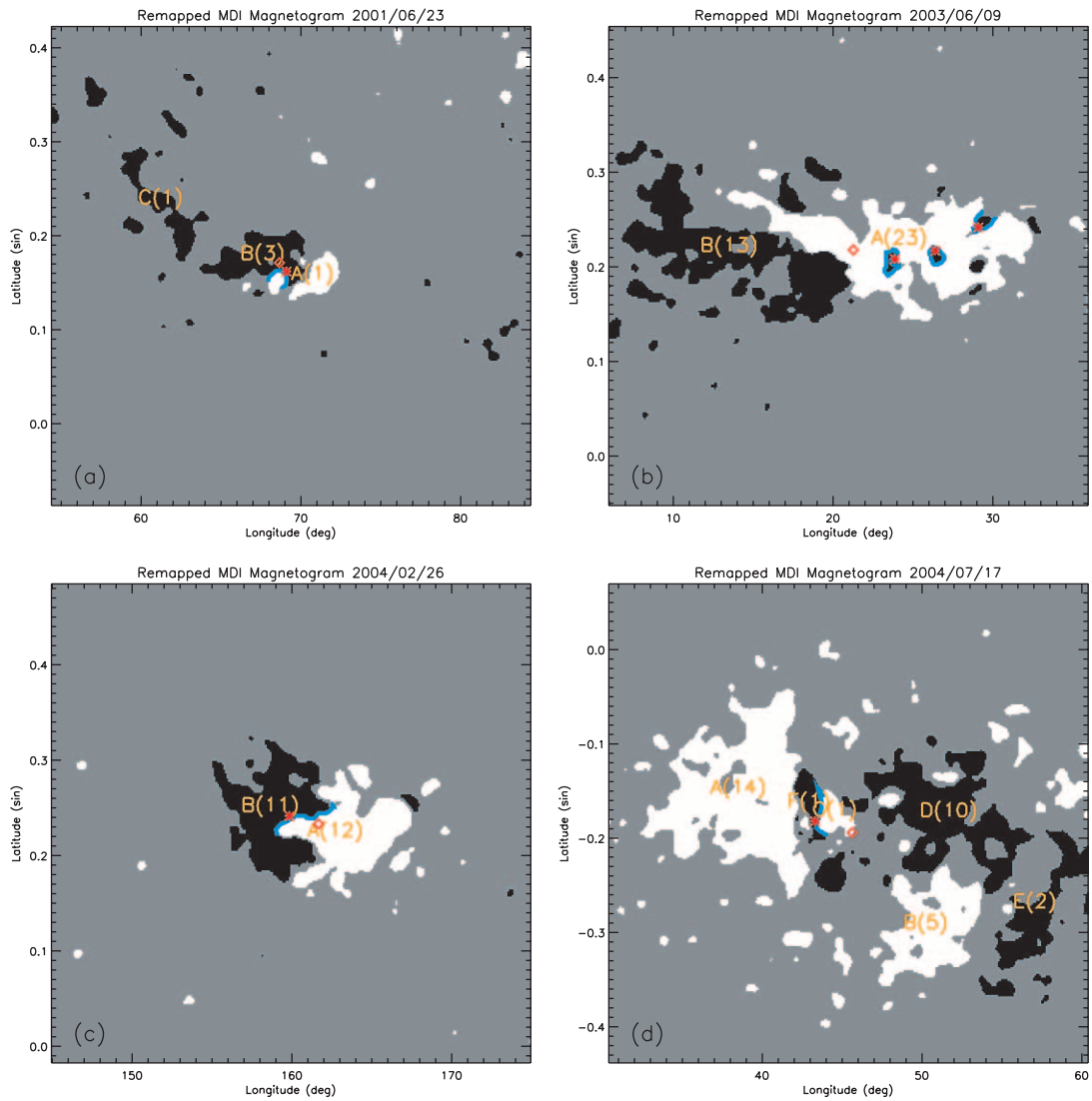

FIG. 3.— Segmented MDI magnetograms for the four confined events, in which strong positive ($\geq$50 G) and negative (≤ -50 G) magnetic fields are highlighted as white and black, respectively. Red asterisks indicate the flare sites, the red diamonds indicate the center of magnetic flux of the active regions, and the blue lines denote the neutral lines over which the flares occurred. (See text for more details.)

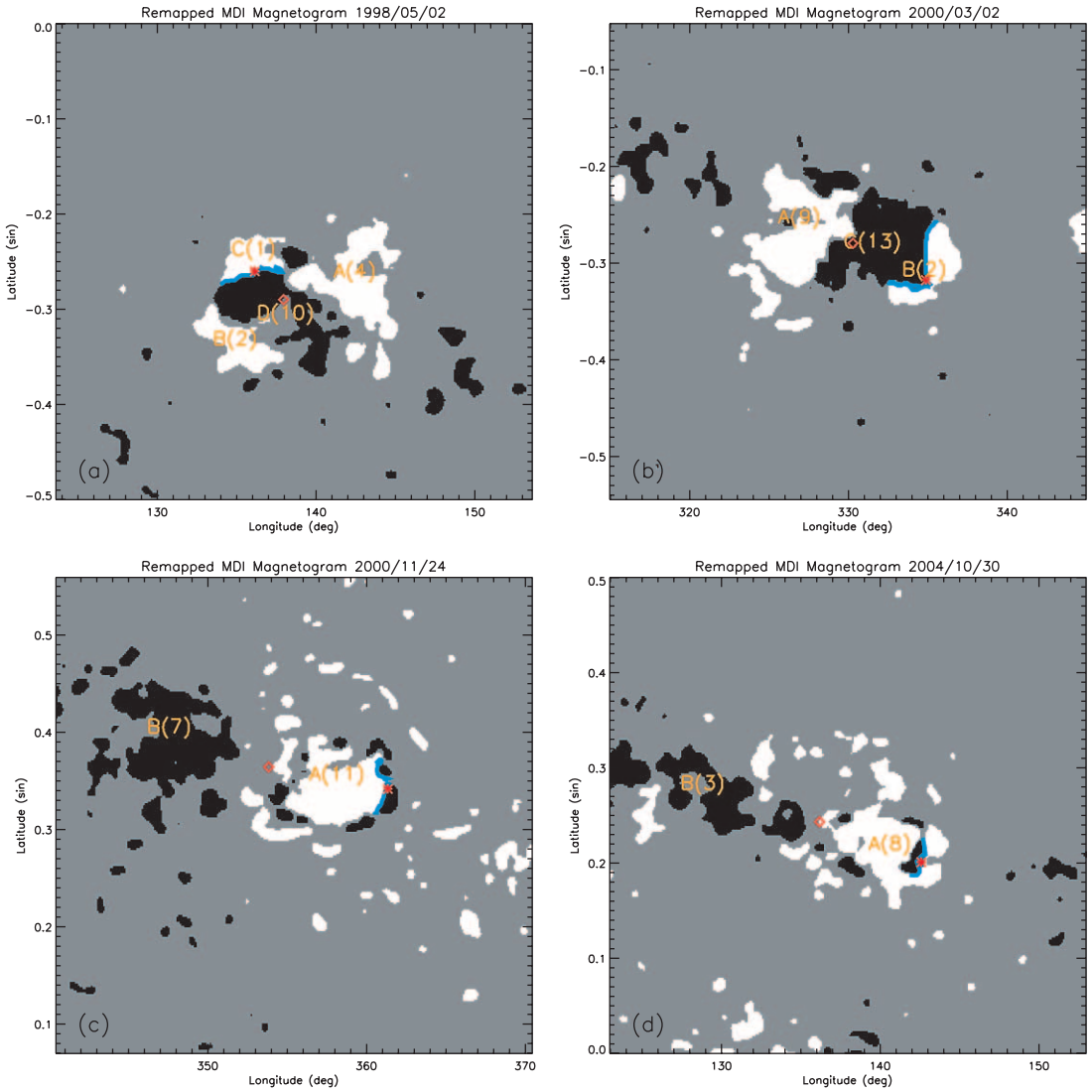

FIG. 4.—Same as Fig. 3, but for the four eruptive events.

TABLE 2

MAGNETIC PROPERTIES OF THE SOURCE ACTIVE REGIONS OF THE CONFINED AND ERUPTIVE FLARES

Event	Date	Flux[a] (10^{13} Wb)	Distance[b] (Mm)
	Confined Flares		
C_1	2001 Jun 23	5	6
C_2	2003 Jun 9	36	17
C_3	2004 Feb 26	23	8
C_4	2004 Jul 17	34	10
	Eruptive Flares		
E_1	1998 May 2	17	22
E_2	2000 Mar 2	24	33
E_3	2000 Nov 24	18	37
E_4	2004 Oct 30	11	29

[a] Total magnetic flux in active regions measured in MDI magnetogram.
[b] Surface distance between the flare site and the center of magnetic flux of the associated active region.

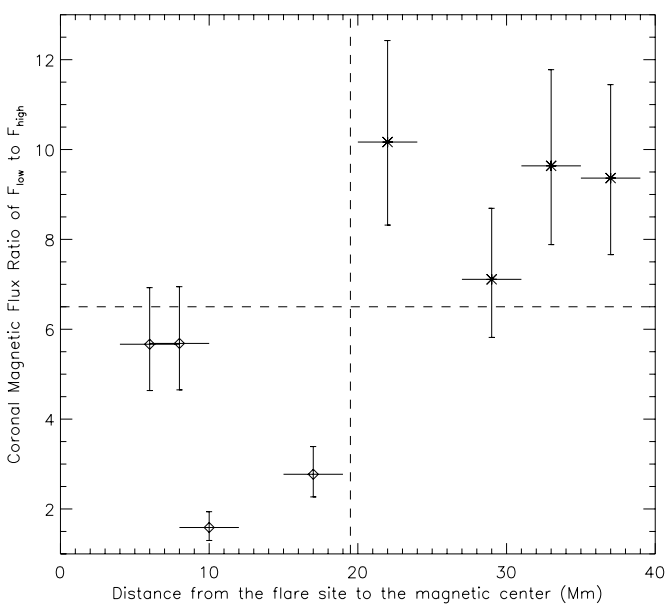

FIG. 5.—Scatter plot showing the magnetic properties of both confined events (*diamonds*) and eruptive events (*asterisks*). The *x*-axis denotes the distance between the flare site and the center of the magnetic flux distribution (COM) of the active region, and the *y*-axis denotes the ratio of magnetic flux in the low and high corona above the neutral line.

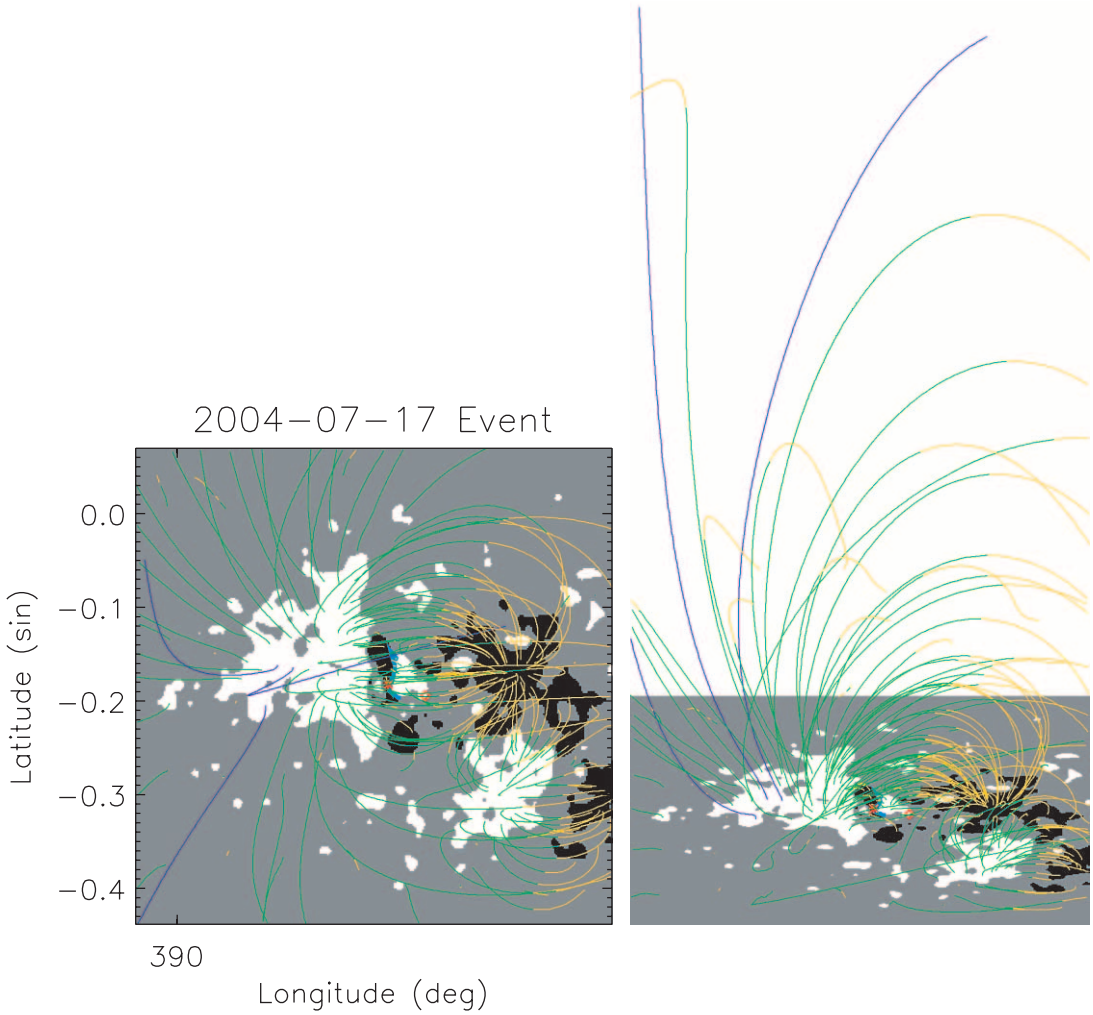

FIG. 6.—Calculated coronal magnetic field of one confined event. The closed field lines are denoted by green and yellow, corresponding to the outward and inward directions, respectively, and the open field lines are shown in blue. The left image is a top view, while the right image is a side view.

We now consider possible errors in calculating the displacement parameter. The error mainly arises from the uncertainty in the recorded weak magnetic field around the active regions. However, in the selected regions of study, which are $30^\circ \times 30^\circ$, the highlighted white and black areas contain about 99% of the total magnetic flux in the region. Therefore, the uncertainty in the flux is expected to be on the order of 1%. Considering the formula for the coordinates of the COM given in the previous paragraph and assuming a typical scale of 100 Mm, the error in the calculated distance is about 1 Mm. Further, considering the spatial resolution of MDI of $\sim$1 Mm (varying from $\sim$0.7 Mm at the central meridian to $\sim$1.4 Mm at a longitude of $\pm 60^\circ$), the overall uncertainty should be about ± 2 Mm. With these considerations, the displacement parameters and their uncertainties are plotted in Figure 5. The confined events are indicated by diamonds, and the eruptive events are indicated by asterisks. The vertical dashed line, which corresponds to a displacement of about 19.5 Mm, effectively separates the two sets of events.

4. MAGNETIC PROPERTIES IN THE CORONA

4.1. *Method*

Having studied the magnetic field distributions in the photosphere, we further look into the magnetic field distributions in the three-dimensional corona. The magnetic field configuration in the corona should ultimately determine eruption or confinement, since the energy releases occur in the corona. There are so far no direct observations of coronal magnetic fields. We have to utilize certain models to calculate the coronal magnetic field based on the observed photospheric boundary. In this paper, we apply the commonly used potential field source-surface (PFSS) model (e.g., Schatten et al. 1969; Hoeksema et al. 1982). The PFSS model is thought to be a useful first-order approximation to the global magnetic field of the solar corona. Nevertheless, we realize that the current-carrying core fields, which are low-lying and near the magnetic neutral line, are far from the potential field approximation; these core fields are likely to be the driving source of any energy release in the corona. Therefore, the use of the PFSS model in this study is limited to calculating the total flux of the overlying large-scale coronal field, which is believed to be closer to a potential approximation. These overlying fields are thought to constrain the low-lying field from erupting.

A modified MDI magnetic field synoptic chart is used as input to our PFSS model. The high-resolution charts[5] are created by interpolating data to disk-center resolution, resulting in a 3600×1080 pixel map. The X- and Y-axes are linear in Carrington longitude (0.1° intervals) and sine of latitude, respectively. This high resolution is useful in creating detailed pictures of the coronal

[5] See http://soi.stanford.edu/magnetic/index6.html.

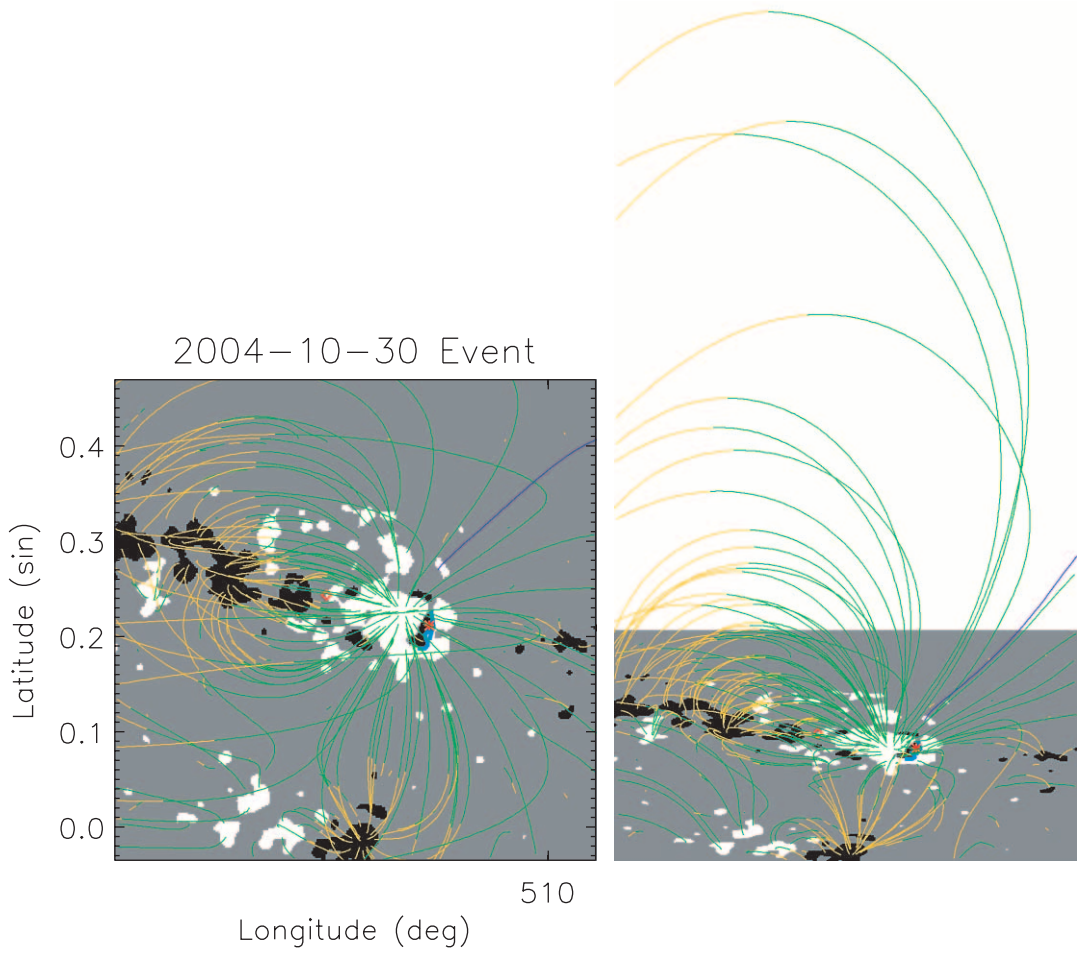

FIG. 7.—Example of an eruptive event, showing the extrapolated magnetic field above the active region.

magnetic field above the source regions of interest. Since an MDI synoptic chart is created from the magnetogram images over a ~27 day solar rotation, the charts do not exactly represent the photospheric magnetic field in the region of interest at the flare/CME time. The details of the source region may be different because of the evolution of the photospheric magnetic field. To mitigate this problem, we use the MDI daily magnetogram to update the original synoptic chart. The process is to remap the snapshot magnetogram image prior to flare occurrence to the Carrington grid and then slice out the region of interest, 30° in longitude and 60° in latitude. This sliced-out region replaces the corresponding portion in the original synoptic chart.

Since the PFSS model makes use of a spherical harmonic series expansion, we realize that high-resolution data require a high-order expansion in order to produce a consistent result. We calculate the spherical harmonic coefficients to as high as 225th order for the input 3600×1080 boundary image. We find that at this order we can obtain the best match between the calculated photospheric magnetic field and the input synoptic chart. The mean value of the difference between them is less than 0.5 G, and the standard deviation is generally $\lesssim$15 G for solar minimum and $\lesssim$25 G for solar maximum, which are comparable to the noise level of MDI magnetograms. This means that we can effectively reproduce the observed photospheric magnetic field with the 225th-order PFSS model. With spherical harmonic coefficients known, it is relatively straightforward to calculate the magnetic field in the three-dimensional volume of the corona.

4.2. *Results*

Figures 6 and 7 show the extrapolated coronal magnetic field lines for one confined event (2004 July 17) and one eruptive event (2004 October 30), respectively. In each figure, the left panel shows the field lines viewed from above, and the right panel shows the field lines viewed from the side by rotating the left panel's view 60° into the page. The green and yellow colors denote closed field lines, with green indicating the loop part of the outward magnetic field (positive magnetic polarity at the footpoints) and yellow the inward field (negative magnetic polarity at the footpoints); blue indicates open field lines. These two examples show that the location of the confined flare, which is near the center of the active region, is covered by a large tuft of overlying magnetic loop arcades, while the location of the eruptive flare, which is near the edge of the active region, has relatively few directly overlying loop arcades. In particular, for the eruptive event the nearby positive and negative magnetic field lines seem to connect divergently with other regions, instead of forming a loop arcade of their own.

To quantify the strength of the overlying field, we calculate the total magnetic flux across the plane with the x-direction extending along the neutral line and the y-direction vertically along the radial direction. The thick blue lines on the photospheric surface in Figures 3 and 4 indicate the neutral lines used in the calculation. The length of the neutral lines is determined, as it encompasses the major part of the eruption region. The overlying magnetic field flux then is normalized to the length of the neutral

TABLE 3
MAGNETIC FLUX PER UNIT LENGTH OVERLYING THE NEUTRAL LINES

Event	Date	F_{total} (10^{10} Wb Mm^{-1})	F_{low} (10^{10} Wb Mm^{-1})	F_{high} (10^{10} Wb Mm^{-1})	F_{low}/F_{high}
		Confined Flares			
C_1	2001 Jun 23	0.40	0.34	0.06	5.67
C_2	2003 Jun 9	0.83	0.61	0.22	2.77
C_3	2004 Feb 26	1.27	1.08	0.19	5.68
C_4	2004 Jul 17	1.19	0.73	0.46	1.59
		Eruptive Flares			
E_1.....	1998 May 2	1.34	1.22	0.12	10.17
E_2.....	2000 Mar 2	1.17	1.06	0.11	9.64
E_3.....	2000 Nov 24	1.14	1.03	0.11	9.36
E_4.....	2004 Oct 30	0.73	0.64	0.09	7.11

line. The normalized overlying magnetic flux thus obtained is a better quantity to use for comparison between different events, because this parameter is not sensitive to the exact length of the neutral lines selected, which may vary significantly from event to event.

Such calculated magnetic fluxes for the eight events are listed in Table 3. In calculating the flux, we do not consider the direction in which the field lines cross over the neutral line. The relative uncertainty of the calculated magnetic flux can be estimated as σ_B/B_0, where σ_B is the uncertainty in the calculated magnetic field strength in the corona and B_0 is the magnetic field strength in the active regions at the photosphere. Considering that σ_B is about 15–25 G, the standard deviation mentioned above, and B_0 is usually hundreds of gauss, we infer that the uncertainty in the overlying magnetic flux is about 10%. This estimate should be true in the case that the coronal magnetic field is correctly obtained by our extrapolation method. If the extrapolated field largely deviates from the real situation, the uncertainty will probably be slightly different.

The total overlying flux, F_{total}, in the height range from 1.0 to 1.5 $R_\odot$, is given in the third column of Table 3. It seems that there is no systematic difference between the confined events and eruptive events. The value for the confined events varies from 0.40×10^{10} to 1.27×10^{10} Wb Mm^{-1}, and that for the eruptive events varies from 0.73×10^{10} to 1.34×10^{10} Wb Mm^{-1}.

We further calculate the flux in two different height ranges, the lower flux from 1.0 to 1.1 $R_\odot$ and the higher flux from 1.1 to 1.5 $R_\odot$. A commonly accepted scenario is that the lower flux should correspond to the inner sheared core field (or a full-fledged flux rope if a filament is present), which tends to move out, while the outer flux is the large-scale overlying arcade, which tends to constrain the inner flux from erupting. Note that the choice of 1.1 $R_\odot$, which corresponds to a height of about 70 Mm above the surface, is rather arbitrary. However, slight changes to this number will not affect the overall results that we reach. The magnetic flux in the low corona, F_{low}, and that in the high corona, F_{high}, are listed in the fourth and fifth columns of Table 3, respectively.

There is a trend that the low-corona flux for the eruptive events is generally larger than that for the confined events. Three out of the four eruptive events have a low-corona overlying flux that is more than 1.0×10^{10} Wb Mm^{-1}, while three out of the four confined events have flux less than 1.0×10^{10} Wb Mm^{-1}. On the other hand, the high-corona flux for the eruptive events seems to be smaller than that for the confined events. Three confined events have high-corona flux greater than 0.15×10^{10} Wb Mm^{-1}, while all four eruptive events have this flux less than 0.15×10^{10} Wb Mm^{-1}.

We further calculate the flux ratio $R = F_{low}/F_{high}$. This quantity is independent of the normalization. It may serve as an index of how weak the constraint on the inner eruptive field is. Interestingly, the flux ratios for the two sets of events fall into two distinct groups. For the confined events, R varies from 1.59 to 5.68, while for the eruptive events, the value of R is larger, from 7.11 to 10.17. The value of 6.5 may be used as a boundary separating the two sets of events. This value probably implies a threshold for confinement or eruptiveness. That is to say, if the flux ratio is less than 6.5, a flare is likely to be confined; otherwise, eruptive. The higher the ratio, the stronger the possibility of a coronal energy release's being eruptive.

5. SUMMARY AND DISCUSSION

In summary, among the 104 X-class flares that occurred during 1996–2004, we found that a total of 11 (~10%) are confined flares without associated CMEs, and all the others (~90%) are eruptive flares associated with CMEs. Four suitable confined flares were selected to make a comparative study with four eruptive flares that are similar in X-ray intensity and duration to those confined events. We have carefully studied the magnetic properties of these events both in the photosphere and in the corona. The following results are obtained:

1. In the photosphere, we cannot find a difference in the total magnetic flux in the surface source regions between the two sets of events. However, there is an apparent difference in the displacement parameter, which we define as the surface distance between the flare site and the center of the magnetic flux distribution. For the confined events, the displacement ranges from 6 to 17 Mm, while for the eruptive events it is from 22 to 37 Mm. This result implies that for an energy release occurring in the center of an active region, it is more difficult to have a complete open eruption, resulting in a flare without a CME. On the other hand, an energy release that occurs away from the magnetic center has a higher probability of producing an eruption, resulting in both flares and CMEs. Whether an eruption can occur or not may be strongly constrained by the overlying large-scale coronal magnetic field. The overlying coronal magnetic field should be strongest and also longest along the vertical direction over the center of an active region. On the other hand, the overlying constraining field should be weaker if the source lies away from the

center. This scenario is further supported by our study of the coronal magnetic field.

2. Calculation of the coronal magnetic field shows that the ratio of the magnetic flux in the low corona to that in the high corona is systematically larger for the eruptive events than for the confined events. The magnetic flux ratio for the confined events varies from 1.6 to 5.7, while the ratio for the eruptive events lies between 7.1 and 10.2. However, there is no evident difference between the two sets of events in the total magnetic flux straddling the neutral lines, and there is only a weak trend indicating a systematic difference in the low- and high-corona magnetic fluxes. This low-to-high coronal magnetic flux ratio serves as a proxy for the strength of the inner core magnetic field, which may play an eruptive role, relative to the strength of the overlying large-scale coronal magnetic field, which may play a constraining role to prevent eruptions. The lower this ratio, the more difficult it is for an energy release in the low corona to be eruptive.

There are a variety of theoretical models of the initiation mechanism of CMEs and the energy release of flares (e.g., Sturrock 1989; Chen 1989; van Ballegooijen & Martens 1989; Forbes & Isenberg 1991; Moore & Roumeliotis 1992; Low & Smith 1993; Mikić & Linker 1994; Antiochos et al. 1999; Lin & Forbes 2000). These models differ in preeruption magnetic configurations, trigger processes, or where magnetic reconnection occurs. Nevertheless, in almost all these models the magnetic configuration involves two magnetic regimes; one is the core field in the inner corona close to the neutral line, and the other is the large-scale overlying, or background, field. The core field is treated as highly sheared or as a full-fledged flux rope; in either case, the core field stores free energy for release. On the other hand, the overlying field is regarded as potential and considered to be the main constraining force preventing the underlying core field from eruption or escape. Török & Kliem (2005) and Kliem & Török (2006) recently pointed out that the decrease of the overlying field with height is a main factor in deciding whether the kink instability (in their twisted flux rope model) leads to a confined event or a CME. On the other hand, Mandrini et al. (2005) reported the smallest CME event ever observed up to 2005, in which the CME originated from a very small source region, a tiny dipole, and developed into a very small magnetic cloud. They suggested that the ejection of tiny flux ropes is possible. Therefore, it is reasonable to argue that the issue of whether an energy release in the corona is eruptive or confined is sensitive to the balance between the inner core field and the outer overlying field. Our observational results seem to be consistent with this scenario.

This study is only a preliminary step to investigate the confinement and/or eruptiveness of solar flares, or coronal energy releases in general. However, it demonstrates that the distribution of magnetic field both in the photosphere and in the corona may effectively provide a clue to the possible nature of an energetic event, whether a flare, a CME, or both. To further evaluate the effectiveness of this methodology, a more robust study involving more events is needed.

We acknowledge the use of the solar data from the LASCO, EIT, and MDI instruments on board the *SOHO* spacecraft. The *SOHO* LASCO data used here are produced by a consortium of the Naval Research Laboratory (US), the Max-Planck-Institut für Aeronomie (Germany), the Laboratoire d'Astronomie (France), and the University of Birmingham (UK). *SOHO* is a project of international cooperation between ESA and NASA. We also acknowledge the use of the CME catalog generated and maintained at the CDAW Data Center by NASA and the Catholic University of America in cooperation with the Naval Research Laboratory, and the solar event reports compiled by the Space Environment Center of NOAA. We are grateful for useful discussion with X.-P. Zhao at Stanford University, who provided the procedures for the PFSS model. This work is supported by NSF SHINE grant ATM 04-54612 and NASA grant NNG05GG19G. Y. W. is also supported by grants from the National Natural Science Foundation of China (40525014) and the Ministry of Science and Technology (2006CB806304), and J. Z. is also supported by NASA grant NNG04GN36G.

REFERENCES

Andrews, M. D. 2003, Sol. Phys., 218, 261
Antiochos, S. K., DeVore, C. R., & Klimchuk, J. A. 1999, ApJ, 510, 485
Brueckner, G. E., et al. 1995, Sol. Phys., 162, 357
Chen, J. 1989, ApJ, 338, 453 (erratum 344, 1051 [1989])
Delaboudinière, J.-P., et al. 1995, Sol. Phys., 162, 291
Feynman, J., & Hundhausen, A. J. 1994, J. Geophys. Res., 99, 8451
Forbes, T. G., & Isenberg, P. A. 1991, ApJ, 373, 294
Green, L. M., Matthews, S. A., van Driel–Gesztelyi, L., Harra, L. K., & Culhane, J. L. 2002, Sol. Phys., 205, 325
Harrison, R. A. 1995, A&A, 304, 585
———. 2003, Adv. Space Res., 32, 2425
Hoeksema, J. T., Wilcox, J. M., & Scherrer, P. H. 1982, J. Geophys. Res., 87, 10331
Kahler, S. W., Sheeley, N. R., Jr., & Liggett, M. 1989, ApJ, 344, 1026
Kliem, B., & Török, T. 2006, Phys. Rev. Lett., 96, No. 255002
Lin, J., & Forbes, T. G. 2000, J. Geophys. Res., 105, 2375
Low, B. C., & Smith, D. F. 1993, ApJ, 410, 412
Mandrini, C. H., Pohjolainen, S., Dasso, S., Green, L. M., Démoulin, P., van Driel–Gesztelyi, L., Copperwheat, C., & Foley, C. 2005, A&A, 434, 725
Mikić, Z., & Linker, J. A. 1994, ApJ, 430, 898
Moore, R. L., & Roumeliotis, G. 1992, in IAU Colloq. 133, Eruptive Solar Flares, ed. Z. Švestka, B. V. Jackson & M. Machado (Lecture Notes in Physics, 399) (New York: Springer), 69
Nindos, A., & Andrews, M. D. 2004, ApJ, 616, L175
Schatten, K. H., Wilcox, J. M., & Ness, N. F. 1969, Sol. Phys., 6, 442
St. Cyr, O. C., & Webb, D. F. 1991, Sol. Phys., 136, 379
Sturrock, P. A. 1989, Sol. Phys., 121, 387
Švestka, Z., & Cliver, E. W. 1992, in IAU Colloq. 113, Eruptive Solar Flares, ed. Z. Švestka, B. V. Jackson & M. Machado (Lecture Notes in Physics, 399) (New York: Springer), 1
Török, T., & Kliem, B. 2005, ApJ, 630, L97
van Ballegooijen, A. A., & Martens, P. C. H. 1989, ApJ, 343, 971
Wang, Y.-M., Ye, P.-Z., Wang, S., Zhou, G.-P., & Wang, J.-X. 2002, J. Geophys. Res., 107(A11), No. 1340
Yashiro, S., Gopalswamy, N., Akiyama, S., Michalek, G., & Howard, R. A. 2005, J. Geophys. Res., 110, No. A12S05
Yashiro, S., Gopalswamy, N., Michalek, G., St. Cyr, O. C., Plunkett, S. P., Rich, N. B., & Howard, R. A. 2004, J. Geophys. Res., 109, No. A07105
Zhang, J., Dere, K. P., Howard, R. A., Kundu, M. R., & White, S. M. 2001, ApJ, 559, 452
Zhang, J., Dere, K. P., Howard, R. A., & Vourlidas, A. 2004, ApJ, 604, 420
Zhou, G., Wang, J., & Cao, Z. 2003, A&A, 397, 1057